IEEE Access
Multidisciplinary ⋮ Rapid Review ⋮ Open Access Journal

Received February 19, 2022, accepted March 1, 2022, date of publication March 8, 2022, date of current version March 16, 2022.

Digital Object Identifier 10.1109/ACCESS.2022.3157868

Modeling and Contouring Control for Cantilever Beam Machine With Structural Flexibility

MENG YUAN[1,2], LEI LI[2], AND ZHEZHUANG XU[1], (Member, IEEE)
[1]College of Electrical Engineering and Automation, Fuzhou University, Fuzhou 350108, China
[2]Rehabilitation Research Institute of Singapore, Nanyang Technological University, Singapore 308232

Corresponding author: Meng Yuan (meng.yuan@ntu.edu.sg)

This work was supported by the Research Funding of the National Natural Science Foundation of China under Grant 61973085.

ABSTRACT In biaxial contouring control applications, the inherent structural flexibility of machines can lead to position discrepancies between the manipulator and actuator, and thus deteriorate the manufacturing performance, especially when the controller is designed without available end-effector side feedback. In this work, we focus on the end-effector contouring control problem for industrial machines with position-dependent flexibility to improve the contouring performance while eliminating the effect of mechanical vibration. A model for the widely used cantilever beam machine is developed to describe the dynamics of the end-effector by capturing the rotation and coupled dynamics between axes. The proposed model is validated through experiment and systematically reduced to switched linear time-invariant models for controller design. By adopting the extended state observer, the proposed control architecture decouples the dynamics between the X and Y-axis and simplifies the controller design process. The model predictive control method is utilised for improving the contouring performance while reducing mechanical vibration. The efficacy of the proposed control framework is demonstrated and validated on the designed high-fidelity model. Performance comparisons between the proposed approach with benchmark controllers are presented.

INDEX TERMS Manufacturing, contouring control, motion control, vibration and noise control.

I. INTRODUCTION

The planar multiaxial movement is involved in industrial machines such as laser profile cutting machines or X-Y positioning systems [1]–[4]. To achieve biaxial manufacturing, the dual-drives gantry (H-frame) machine and the cantilever beam (T-frame) machine are widely used [5]. The cantilever beam machine involves two actuators driving in perpendicular axes. The one end on the Y-axis supports the other end of the X-axis to move along the beam. The coordinated motion of the two axes ensures the moving of the end-effector to the desired position in two-dimensional space [6]. Structures of machines were traditionally considered rigid at a time when structural components were heavy and accuracy was not highly regarded [7]–[9]. However, the flexible linkages in machines lead to position discrepancies between actuators and the end-effector due to their non-rigid characteristics, thus deteriorating the manufacturing performance [9].

To eliminate the detrimental effect caused by vibration in machines, methods including structure stiffness enhancement and controller design have been investigated by researchers and engineers in fields including microelectromechanical systems [10], robotics [11], and space systems [12]. In terms of stiffness enhancement for contouring applications, the dual-drives gantry machine is introduced to improve the rigidity of systems by adding another motor on the parallel slides [13]. However, the effect of vibration is only reduced instead of eliminated by changing the system structure. Therefore, instead of modifying the structure of machines, designing advanced control algorithms are essential in eliminating the mechanical oscillation during the contouring process, and establishing an accurate model with the consideration of structural flexibility becomes the prerequisite for a proper controller [14]–[16].

Some efforts have been devoted to the modelling of industrial contouring machines with structural flexibility [17]–[19]. Although the varying dynamic resonance was considered for an XY table in [17], the system model was established based on the frequency response at different points and an analytical model is not formed. In [18], the model of end-effector linked by a flexible beam was proposed and tip tracking control results were presented. The model of dual-drive gantry

The associate editor coordinating the review of this manuscript and approving it for publication was Okyay Kaynak.

machine with structural flexibility was investigated in [19] and the control-oriented model was used for synchronisation control. However, the position-dependent flexibility was not considered in [18] and [19], which is not consistent with real applications.

At the same time, a large number of effort has been devoted to the development of advanced control algorithms for the improvement of contouring accuracy [20]–[22]. In [20], the variable-gain cross-coupling controller was proposed to explicitly reduce the contouring error. The adaptive robust control method was implemented with multiple task coordinates on a gantry machine for contouring control in [21]. In [22], the feedforward computed torque (FFCT) control was investigated for a three-axis manipulator. It was shown that both the tracking and contouring performance were improved compared to proportional-integral-derivative (PID) with an observer and conventional PID control. However, the system constraints including state and input constraints are not explicitly considered in these works.

Hence, it is necessary to establish a dynamic model that can precisely describe the end-effector position, and advanced control methods that can explicitly ensure the operating constraints while enhancing the contouring performance for machines with structural flexibility are required. For systems with position-dependent flexibility, the dynamics is coupled that complicates the controller design [12]. To eliminate the unmodelled disturbance or nonlinearities, methods including the disturbance observer-based methods were investigated [23], [24]. The related work of observer-based control can be found in motion control applications including the motor control [25]–[28], machine tools [29] and XY tables [30], [31]. The model predictive control (MPC) serves as an attractive approach for explicitly taking account of the constraints in the motion control. In [32] and [33], the MPC-based position and speed control are designed for the two-mass-drive system. For machines with structural flexibility, the MPC based error bounded tracking was proposed in [34].

Considering the cantilever beam machine is still widely adopted since it has fewer parts and lower cost compared to a gantry machine, in this work, the dynamic modelling and contouring control for the cantilever beam machine is investigated. We focus on the end-effector contouring control problem for industrial machines with position-dependent flexibility to improve the contouring performance while eliminating the effect of mechanical vibration. The contribution of this work involves two parts. The first part is the system modelling:

1) A high-fidelity model is proposed for the cantilever beam machine system to capture the dynamics of end-effector with rotation and coupled dynamics between axes.
2) The proposed model is not only a theoretical outcome but also is validated based on experiment results.

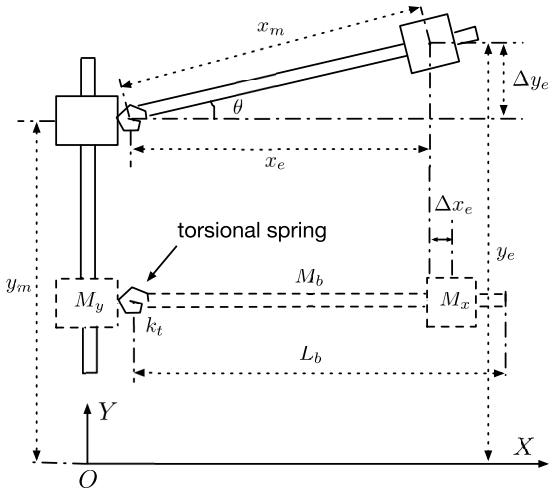

FIGURE 1. Schematic diagram of torsional spring based vibration model.

3) The proposed model can be easily extended to other biaxial systems with the consideration of fundamental vibration mode.

The second part of contributions is the designed contouring control framework:

1) The proposed control architecture decouples the dynamics between axes and simplifies the controller design process based on the extended state observer (ESO).
2) The model predictive control method is adopted to improve the contouring performance while eliminating the effect of vibration in the optimisation problem.
3) The proposed control framework for solving the contouring problem using the switched linear-time invariant (LTI) model can be applied to other systems with coupled dynamics.

Notation: $\mathbb{R}$ is the set of real integer numbers. $\mathbb{Z}_{[m,n]}$ is the set of integers range from m to n with m, n included. Consider $a \in \mathbb{R}^{n_a}$, $b \in \mathbb{R}^{n_b}$, the stacked vector is represented as $(a, b) \triangleq [a^T, b^T]^T \in \mathbb{R}^{n_a+n_b}$.

II. SYSTEM MODELLING AND MODEL VALIDATION

A. STRUCTURAL CONFIGURATION

In motion control, the closed-loop bandwidth of systems is limited by the first few vibration modes [18]. To achieve a trade-off between the accuracy and complexity of modelling, a torsional spring-based model is proposed to describe the position of the end-effector in a cantilever beam machine with the consideration of fundamental vibration resonance.

The schematic diagram of the model is given in Fig. 1 where the dashed line depicts the machine in steady-state and the solid line shows the machine in moving conditions. The structural flexibility of the system is represented by a virtual torsional spring that links the slide and flexible beam, and the change of vibration frequency is captured when the end-effector moves. The torsional spring with stiffness coefficient k_t introduces another degree of freedom for the rotation

dynamics. In Fig. 1, the notations x_m, y_m are the positions of X and Y-axis motors respectively, which are measurable; x_e, y_e are the position components of the end-effector, which are not measurable, θ is the angle formed due to deformation. The discrepancy errors on X and Y-axis are denoted by $\Delta x_e = |x_m - x_e|$ and $\Delta y_e = |y_m - y_e|$.

B. LAGRANGIAN-BASED SYSTEM MODELLING

To derive the equations of motion for this cantilever beam model, the Lagrangian based modelling is conducted [22]. The Lagrange equation is:

$$\frac{d}{dt}\left(\frac{\partial L}{\partial \dot{\mathbf{q}}}\right) - \frac{\partial L}{\partial \mathbf{q}} = W, \tag{1}$$

where $L = K - P$ is a Lagrangian, W is a vector of generalised force (or moments) acting in the direction of generalising the coordinate $\mathbf{q}$. For the proposed torsional spring based model, the generalising coordinate is $\mathbf{q} = [x_m, y_m, \theta]^T$.

The kinetic and potential energies of the investigated system are given by the sum of energies from its components including the X and Y-axis motors and torsional spring with the beam as:

$$K = K_1 + K_2 + K_3, \tag{2}$$
$$P = P_1 + P_2 + P_3, \tag{3}$$

where K and P are the kinetic and potential energy of the system, K_1, P_1 are the kinetic and potential energies of the X-axis motor; K_2, P_2 are the kinetic and potential energies of the Y-axis motor; K_3, P_3 are the kinetic and potential energies of the cantilever beam and spring. Explicitly,

$$K_1 = \frac{1}{2}M_x\left(\dot{x}_e^2 + \dot{y}_e^2\right), \tag{4}$$
$$K_2 = \frac{1}{2}M_y\dot{y}_m^2, \tag{5}$$
$$K_3 = \frac{1}{2}M_b\left(\dot{x}_b^2 + \dot{y}_b^2\right) + \frac{1}{2}I_b\dot{\theta}^2, \tag{6}$$
$$P_1 = 0,\ P_2 = 0,\ P_3 = \frac{1}{2}k_t\theta^2, \tag{7}$$

where M_x and M_y are the mass of the X and Y-axis motors respectively, M_b is the mass of the beam, x_b, y_b are the position projections from the centre of mass of the beam onto the X and Y-axis respectively, I_b is the moment of inertia of the beam calculated at the centre of the mass of the beam.

Considering the material of the beam is equally distributed, the position (x_b, y_b) and moment of inertia at the centre of mass of the beam I_b are calculated as,

$$x_b = \frac{L_b}{2}\cos\theta, \tag{8}$$
$$y_b = y_m + \frac{L_b}{2}\sin\theta, \tag{9}$$
$$I_b = \frac{M_bL_b^2}{12}, \tag{10}$$

where L_b is the length of the flexible beam. The Lagrange of the system is given by

$$L = K_1 + K_2 + K_3 - P_1 - P_2 - P_3. \tag{11}$$

According to Eq. (1), we have the Lagrange equations by differentiating the Lagrange with respect to $\dot{\mathbf{q}}$ and $\mathbf{q}$ as:

$$\frac{d}{dt}\left(\frac{\partial L}{\partial \dot{x}_m}\right) - \frac{\partial L}{\partial x_m} = k_x i_x, \tag{12}$$
$$\frac{d}{dt}\left(\frac{\partial L}{\partial \dot{y}_m}\right) - \frac{\partial L}{\partial y_m} = k_y i_y, \tag{13}$$
$$\frac{d}{dt}\left(\frac{\partial L}{\partial \dot{\theta}}\right) - \frac{\partial L}{\partial \theta} = -c_t\dot{\theta}, \tag{14}$$

Or explicitly,

$$M_x\left(\ddot{x}_m + \ddot{y}_m\sin\theta - \dot{\theta}^2x_m\right) = k_x i_x, \tag{15}$$
$$M_t\ddot{y}_m + \frac{M_bL_b}{2}(\ddot{\theta}\cos\theta - \dot{\theta}^2\sin\theta) + M_x(\ddot{x}_m\sin\theta + 2\dot{x}_m\dot{\theta}\cos\theta + x_m\ddot{\theta}\cos\theta - x_m\dot{\theta}^2\sin\theta) = k_y i_y, \tag{16}$$
$$\frac{M_bL_b^2}{3}\ddot{\theta} + \frac{M_bL_b}{2}\ddot{y}_m\cos\theta + M_x\left(x_m^2\ddot{\theta} + 2x_m\dot{x}_m\dot{\theta} + x_m\ddot{y}_m\cos\theta\right) + k_t\theta = -c_t\dot{\theta}, \tag{17}$$

where $M_t \triangleq M_x + M_y + M_b$ is the total mass; k_x, k_y are the force constants of X and Y-axis motors; i_x and i_y are the currents generated by X and Y-axis motors respectively; c_t is the damping coefficient of the torsional spring.

The position of the end-effector is calculated in the form of coordinate $\mathbf{q}$ as:

$$x_e = x_m\cos\theta, \tag{18}$$
$$y_e = y_m + x_m\sin\theta. \tag{19}$$

In this work, the investigated contouring problem is designing a control law $u = (i_x, i_y)$ for systems with dynamics Eq. (15), Eq. (16) and Eq. (17) such that the system states $x_e \to x_m = x_e^*$, $y_e \to y_m = y_e^*$ and $\theta \to 0$, where x_e^* and y_e^* are the desired positions of end-effector on X and Y-axis.

III. CONTROLLER DESIGN

In this section, the proposed high-fidelity model is utilised for the model-based contouring control design. The derivation of control-oriented modelling and the proposed control framework are presented.

A. CONTROL ORIENTED MODELLING

The dynamic equation Eq. (15) can be reformulated as Eq. (20) by lumping all the terms involving y_m, θ as disturbance term:

$$M_x\ddot{x}_m = k_x i_x + F_{dx}, \tag{20}$$

where $F_{dx} = -M_x\left(\ddot{y}_m\sin\theta - \dot{\theta}^2x_m\right)$. The idea of merging the term including y_m and θ is to decouple the axes controller and simplify the controller design process based on the fact the magnitude of this nonlinear term is bounded and converges to zero as $\theta \to 0$ and $\dot{\theta} \to 0$ during the control process. The design of ESO later estimates this nonlinear part and cancels the effect by introducing the correction term at the current loop level.

The Eq. (16) and Eq. (17) are approximated at different operating points $\bar{x}_m$ to cancel the dependence of x_m dynamics, and the equations are organised with a small angle approximation as:

$$\left(M_x + M_y + M_b\right)\ddot{y}_m + \left(\frac{M_b L_b}{2} + M_x \bar{x}_m\right)\ddot{\theta} = k_y i_y + F_{d1}, \tag{21}$$

$$\left(\frac{M_b L_b}{2} + M_x \bar{x}_m\right)\ddot{y}_m + \left(\frac{M_b L_b^2}{3} + M_x \bar{x}_m^2\right)\ddot{\theta} + c_t\dot{\theta} + k_t\theta = F_{d2}, \tag{22}$$

where the lumped terms include the nonlinear coupling between states as $F_{d1} = \frac{M_b L_b}{2}\dot{\theta}^2\theta - M_x(\ddot{x}_m\theta + 2\dot{x}_m\dot{\theta} - \bar{x}_m\dot{\theta}^2\theta)$ and $F_{d2} = -2M_x\bar{x}_m\dot{x}_m\dot{\theta}$.

For the Y-axis motor control, the discrete-time state space model is derived from Eq. (21) and Eq. (22) with given sampling time T_s as:

$$\xi(k+1) = A(\bar{x}_m)\xi(k) + B(\bar{x}_m)i_y(k) + E(\bar{x}_m)F_{dy}(k) \tag{23}$$

where $\xi(k) \triangleq [y_m(k), \dot{y}_m(k), \theta(k), \dot{\theta}(k)]^T$ denotes the state; $F_{dy}(k) \triangleq [F_{d1}(k), F_{d2}(k)]^T$ is the vector of lumped nonlinear couplings. The coefficient matrices $A(\bar{x}_m)$, $B(\bar{x}_m)$ and $E(\bar{x}_m)$ are position-dependent and can be inferred from Eq. (21) and Eq. (22). The detailed structure of the coefficient matrices are given in the appendix. It has to be noticed that Eq. (23) is linearised at different $\bar{x}_m$ point. With larger numbers of chosen $\bar{x}_m$, the model mismatch between the linearised model Eq. (23) and its nonlinear form is smaller, but it comes with the cost at more frequent controller switching and higher computation load.

B. PROPOSED CONTROL STRUCTURE

The diagram of the entire control architecture and plant is demonstrated in Fig. 2. To eliminate the effect caused by nonlinear coupling F_{dx} in Eq. (20), the ESO is introduced with conventional cascaded architecture for the X-axis motor control. The MPC based approach is designed based on the switched linear time-invariant model Eq. (23) to control the movement of the Y-axis motor while reducing the oscillation during the process.

For X-axis motion control, we define the state of the ESO as $\hat{x} = [\hat{x}_m, \hat{v}_m, \hat{\zeta}_m]^T$, where $\hat{x}_m$ is the estimate of X-axis position, $\hat{v}_m$ is the estimate of X-axis velocity and $\hat{\zeta}_m$ is the estimate of the lumped nonlinear part F_{dx}. The dynamics of ESO is designed as:

$$\begin{aligned}
\dot{\hat{x}}_m &= \hat{v}_m + \frac{3}{\delta}\left(x_m - \hat{x}_m\right) + \delta\Phi\left(\frac{x_m - \hat{x}_m}{\delta^2}\right) \\
\dot{\hat{v}}_m &= \frac{k_x}{M_x}i_x + \frac{3}{\delta^2}\left(x_m - \hat{x}_m\right) + \hat{\zeta}_m \\
\dot{\hat{\zeta}}_m &= \frac{1}{\delta^3}\left(x_m - \hat{x}_m\right)
\end{aligned} \tag{24}$$

where $\hat{\zeta}_m \triangleq \frac{\hat{F}_{dx}}{M_x}$ induces an estimate of F_{dx}, δ is the only tuning parameter of the ESO. The nonliear function Φ is chosen as the same function in [35], as:

$$\Phi(r) = \begin{cases} -\frac{1}{4}, & r \in \left(-\infty, -\frac{\pi}{2}\right], \\ \frac{1}{4}sinr, & r \in \left(-\frac{\pi}{2}, \frac{\pi}{2}\right], \\ \frac{1}{4}, & r \in \left(\frac{\pi}{2}, +\infty\right). \end{cases} \tag{25}$$

The designed ESO follows the general structure of the nonlinear extended state observer in [35] to ensure the convergence of the designed ESO. The convergence rate is presented by the limit superior of the estimation error sequence as $\lim_{t\to\infty}\sup|F_{dx}(t)/M_x - \hat{\zeta}_m(t)| \leq \mathcal{O}(\delta)$.

By introducing $-\frac{M_x}{k_x}\hat{\zeta}_m$ term into the current reference for X-axis motor, the effect of nonlinear coupling F_{dx} is cancelled. With the given position reference x_e^* and system feedback including x_m, $\dot{x}_m$ and i_x, the control law for the X-axis is:

$$\begin{aligned}
i_x &= f(x_e^*, x_m, \dot{x}_m, i_x) \\
&= k_{pv}e_v + \frac{k_{pv}}{T_{iv}}\int e_v dt - \frac{M_x}{k_x}\hat{\zeta}_m,
\end{aligned} \tag{26}$$

where $e_v = k_{pp}(x_e^* - x_m) - \dot{x}_m$ is the velocity error, k_{pp} is the gain of proportional controller in the position loop, k_{pv} is the proportional gain and T_{iv} is the integral time constant of PI controller in the speed loop.

In industrial manufacturing, the time-stamped reference is generally provided. The reference for Y-axis controller is $r(k) = \left[y_m^*(k), \dot{y}_m^*(k), \theta^*(k), \dot{\theta}^*(k)\right]^T$, where $\theta^*(k) = \dot{\theta}^*(k) = 0$ is for oscillation reduction in this application. With N steps pre-known reference trajectory $\gamma^N(k) = (r(k), \cdots, r(k+N-1))$, the Y-axis control input is computed by solving the following optimisation problem at each time instant:

$$\begin{aligned}
U^*(k) = \arg\min_{U(k)} &\sum_{i=0}^{N-1}\left(\|r(k+i) - \xi(i)\|_Q^2 + Ri_y^2(k)\right) \\
&+ \|r(k+N) - \xi(N)\|_P^2 \\
s.t.\ &\xi(i+1) = A(\bar{x}_m)\xi(i) + B(\bar{x}_m)i_y(i), \\
&i_y(i) \in \mathcal{U}, \quad \forall i \in \mathbb{Z}_{[0,N-1]}, \\
&\xi(0) = \xi(k)
\end{aligned} \tag{27}$$

where $U(k) = \left(i_y(0), \cdots, i_y(N-1)\right)$; $\|x\|_Q^2 \triangleq x^T Q x$; Q and R are the weighting coefficients which emphasise the tracking performance and control effort respectively. The compact set $\mathcal{U}$ describes the constraint of the control input. The first component of $U^*(k)$ is applied to the plant at each time instant as the Y-axis control law, i.e. $i_y(k) = i_y^*(0)$. The inclusion of the terminal cost in the Eq. (27) ensures the stability of the controller. The value of coefficient P is computed based on the discrete-time algebraic Riccati equation with the chosen values of Q, R and nominal system model [36].

For dealing with the nonlinearities in the system, the following remark is given:

Remark 1: With the explicit expression of F_{dx}, F_{d1} and F_{d2} in Eq. (20), Eq. (21) and Eq. (22), all the nonlinearities

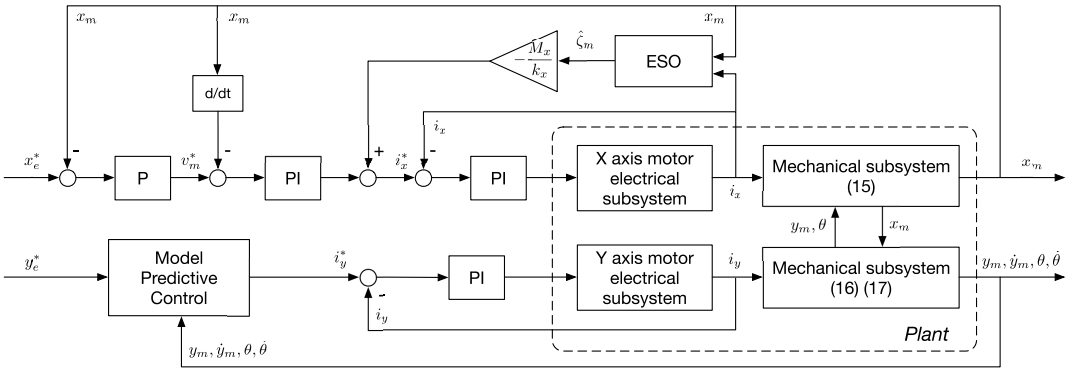

FIGURE 2. Schematic diagram of the proposed control architecture and system.

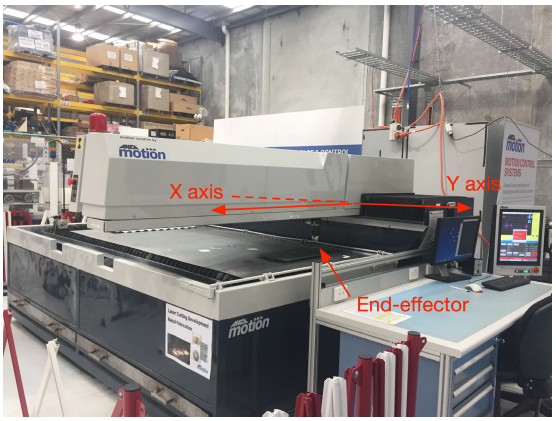

FIGURE 3. Cantilever beam machine used for model validation.

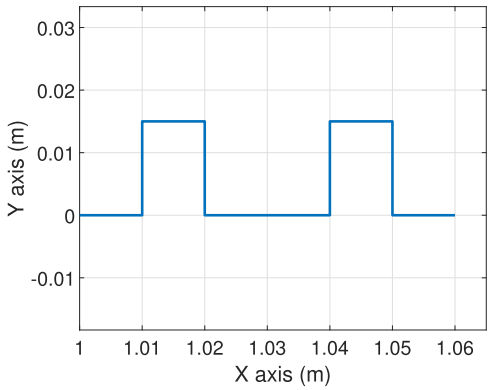

FIGURE 4. Reference path for the model validation of biaxial laser cutting machine.

are assumed within bounded disturbance sets considering the states of the system are bounded. The fast convergence of the designed ESO provides the estimation $\hat{F}_{dx}$ for decoupling the controller design between axes. For the nonlinearities in Eq. (23), the values of F_{d1} and F_{d2} converge to zeros considering $\dot{\theta} \to 0$ and $\theta \to 0$. During the contouring process, the bounded disturbances F_{d1} and F_{d2} are handled by the MPC-based feedback control.

IV. RESULTS

To validate the proposed model, we conduct the model validation on an industrial laser cutting machine. The efficacy of the designed control architecture is presented by the simulated contouring control on the high-fidelity model.

A. MODEL VALIDATION

The industrial machine investigated is a laser cutting machine in the cantilever beam frame as shown in Fig. 3. Two rotary permanent magnet synchronous motors with rack and pinion transmission parts are mounted on the slide and beam with mass 70 kg and 180 kg respectively. The length of the beam is 2.5 m. Two encoders are installed on the feed drives to provide the position feedback for the servo drive.

Since there is no direct feedback from the end-effector, the model validation is conducted by comparing the contour generated by the high-fidelity model with the practical laser cutting workpiece. The conventional cascaded control architecture is utilised here for the model validation purpose.

The cantilever beam machine is required to track a desired path as shown in Fig. 4 with a maximum acceleration at 2 m/s^2 and maximum velocity at 2 m/s. The amplitude and frequency of the reference are carefully chosen to fully excite the system. The end-effector starts moving from $(x_e, y_e) = (1, 0)$ instead of $(x_e, y_e) = (0, 0)$ since the oscillation is more obvious when the end-effector is moving away from the Y-axis.

The contouring path generated by the proposed high-fidelity model is given in Fig. 5 and the corresponding laser cutting result is shown in Fig. 6. From Fig. 5, it can be seen that both the motor and end-effector positions follow the given reference while obvious oscillation occurs at the end-effector side. By comparing the highlighted part in Fig. 5 with the cutting result in Fig. 6, we can see that the vibration observed in the experiment is precisely captured by the proposed model.

The trajectories of the motor and end-effector on X and Y-axis are given in Fig. 7a and Fig. 7b respectively. The results show that the error discrepancy Δy_e on Y-axis is larger than the error Δx_e on X-axis. This is due to the fact that $\Delta x_e = |x_m(1 - \cos\theta)| \to 0$ and $\Delta y_e = |x_m \sin\theta| \to |x_m\theta|$ when the rotation angle θ is small. The error discrepancy Δy_e

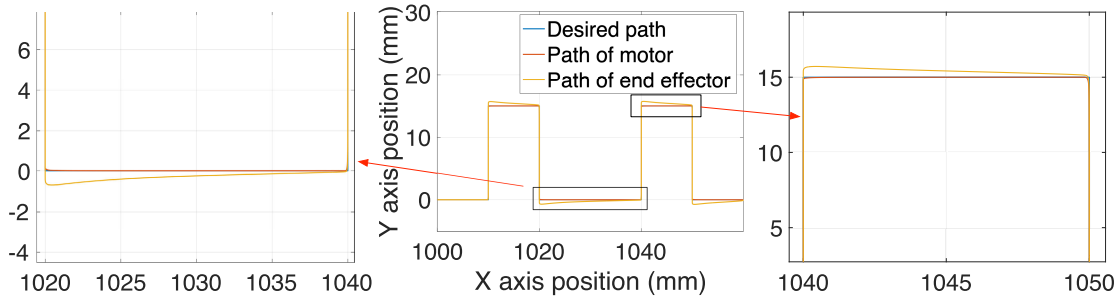

FIGURE 5. Contouring path generated by the proposed model.

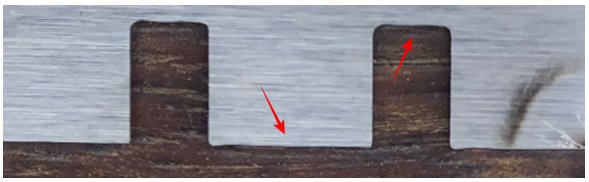

FIGURE 6. Contour of laser cutting workpiece.

leads to a large tracking error on the Y-axis, resulting the contouring error that can be seen in Fig. 5 and Fig. 6.

B. CONTOURING CONTROL BASED ON THE PROPOSED CONTROL METHOD

In practical contouring control, the desired contour is generally a combination of circular and straight lines. To validate the effectiveness of our proposed control framework, we require the end-effector to follow a contour consisting of a circular path with a 0.05 m radius and straight lines for acceleration and deceleration. The maximum velocity of reference is 0.5 m/s and the maximum acceleration is 5 m/s^2. The whole contouring control simulation is conducted based on the verified high-fidelity model with the consideration of discretisation. The desired trajectories on the X and Y-axis as well as the desired path are shown in Fig. 8.

For the tuning of X-axis control law Eq. (26), the proportional gain in the position loop is chosen as $k_{pp} = 200$ 1/s. The proportional gain and integral time constant in the velocity loop are $k_{pv} = 154$ As/m and $T_{iv} = 5$ s. The observer gain in ESO is chosen as $\delta = 0.001$ to ensure the fast convergence of disturbance estimation while avoiding the potential sharp spike. Since the design of the current loop is not the focus of this work, the detail is not covered. The values of the proportional gain and integral time constant in the current loop are given here for the reader's convenience as $k_{pc} = 7$ V/A and $T_{ic} = 0.52$ ms. The tuning of the current loop ensures the time scale separation between the electrical and mechanical subsystems.

For the Y-axis controller, the switching LTI model Eq. (23) is linearised at $\bar{x}_m = \{0.025, 0.075\}$ m points to achieve a trade-off between the accuracy of the control-oriented model and numbers of controller switching. The weighting matrix Q in the MPC formulation Eq. (27) is chosen as diagonal matrix with entries as $\{1000, 1000, 100, 0\}$ and $R = 0.001$ is

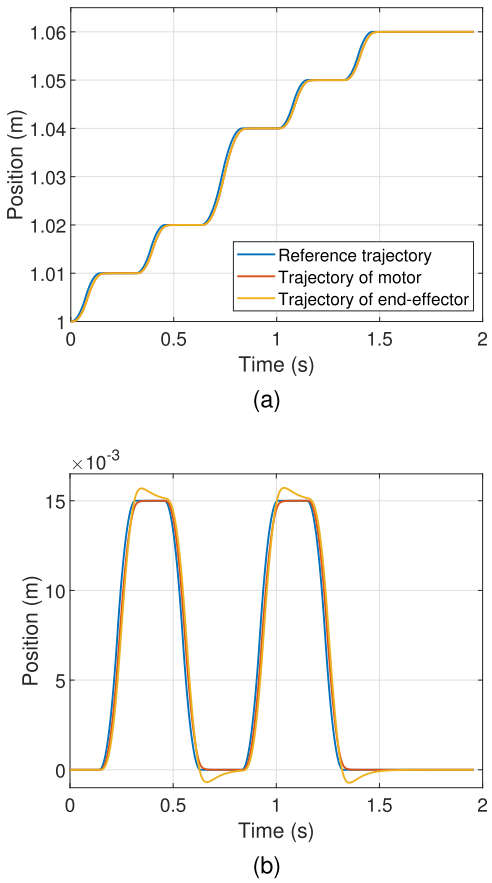

FIGURE 7. Trajectory of laser cutting machine for model validation: (a) X axis, (b) Y axis.

selected. The value of the P matrix is computed by the corresponding discrete-time algebraic Riccati equation. The prediction and control horizon are chosen as the same value $N = 6$. The sampling rate of the MPC is 1 ms.

The designed ESO is used to estimate the lumped nonlinear term F_{dx} to decouple the system dynamics. The observation accuracy directly influences the tracking result on the X-axis and the ultimate contouring performance. With the explicit form of the lumped term F_{dx}, the actual value of F_{dx} in the simulation and the estimated value $\hat{F}_{dx}$ from the ESO are demonstrated in the Fig. 9. It can be seen that obvious noise exists in F_{dx} during 0.3 to 0.4 s and 0.5 to 0.7 s. This is due

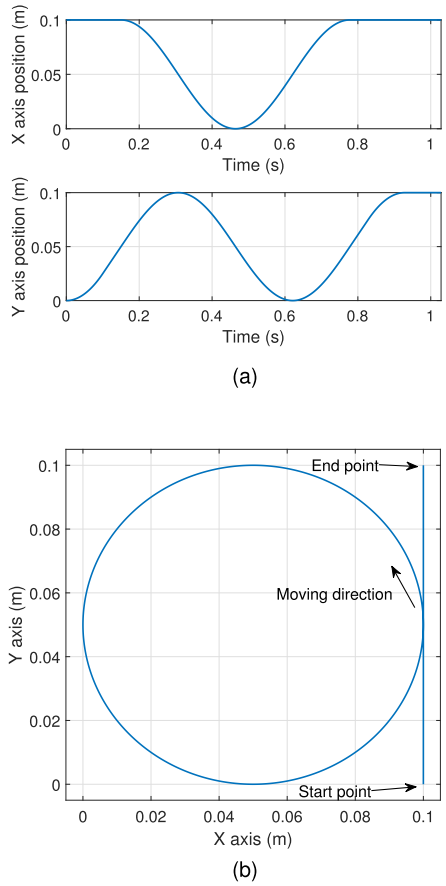

FIGURE 8. Desired reference: (a) time-dependent trajectory on X and Y axes; (b) contour.

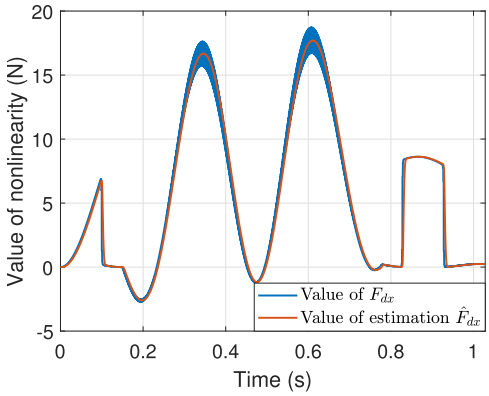

FIGURE 9. Performance of the designed ESO.

to the double derivative term $\ddot{y}_m$ in the F_{dx} when y_m changes fast during that period. The noise in F_{dx} hinders the use of methods such as feedback linearisation. The observation $\hat{F}_{dx}$ from the designed ESO precisely capture the actual value of this lumped disturbance. This estimated value is used in the current reference as shown in Eq. (26) to decouple the dynamics between axes.

The tracking errors of the end-effector on X and Y-axis, i.e., $(x_e^* - x_e)$ and $(y_e^* - y_e)$, are shown in Fig. 10. Since only straight lines and a circle are included in the desired path, the

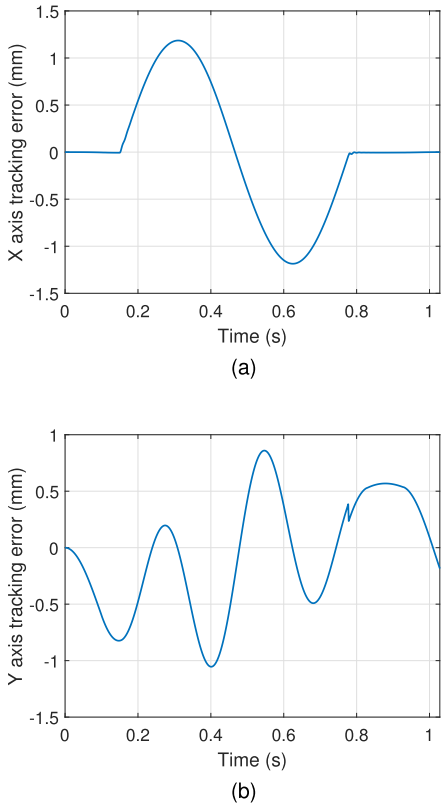

FIGURE 10. Tracking error during the contouring process: (a) X axis; (b) Y axis.

contouring error can be explicitly calculated and is illustrated in Fig. 11. On the first straight line segment from 0 to 0.15 s, the non-zero tracking error on Y-axis leads to a zero contouring error. This is due to the fact that the end-effector starts on the contour and there is no displacement on the X-axis. On the circular path, the tracking error on X-axis fluctuates when the reference accelerates and decelerates correspondingly, leading to a tracking error in sinusoidal form due to the reactive characteristics of the PI controller. Although the tracking errors on the X and Y-axis increase from 0.2 to 0.3 s, the mapped contour is projected and it results in a local minimum around 0.3 s. This pattern continues for the rest of the circular contour. After around 0.77 s, the straight line becomes the desired contour and the tracking error on the X-axis maps directly to the contouring error. The maximum contouring error is around 1.33 mm, which is only 2.8% of the circular radius.

Considering the conventional cascaded control is still the most widely adopted control algorithm in practical motion control field [37], it is selected as one of the benchmark controllers for performance comparison in this study. The cascaded controller is utilised in the two axes for the trajectory tracking and the values of tuning parameters are chosen as the same numbers used in the proposed X-axis PI controller for a fair comparison.

The linear quadratic regulator (LQR) controller is used as another benchmark controller to investigate the performance

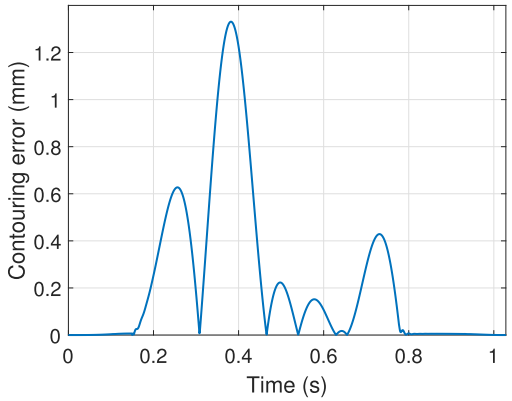

FIGURE 11. Contouring error during the whole process based on the proposed control architecture.

of optimal controller in contouring control for system with operating constraint and structural flexibility. The LQR controller is designed based on the assumption that the system structure is solid and the rotation dynamics is ignored. The quadratic cost function for the X and Y-axis is $J_j = \xi_j^T Q_j \xi_j + R_j i_j^2$ with $j = \{x, y\}$, where $\xi_x \triangleq (x_m, \dot{x}_m)$ and $\xi_y \triangleq (y_m, \dot{y}_m)$. The tuning parameters Q_x and Q_y are chosen as diagonal matrices with entries as $\{30, 30\}$ and $R_x = R_y = 0.1$ are selected to achieve an acceptable contouring performance.

For the proposed control framework, the PI controller can be replaced by any other advanced control methods with the designed extended state observer for X-axis movement control. Similarly, the general MPC for Y-axis movement can be replaced by algorithms such as robust MPC or adaptive MPC if robustness or parameter uncertainties are the concerns. The comparison presented here is for showing the efficacy of the proposed control framework in dealing with systems with coupled and rotation dynamics in contouring applications.

The tracking errors $|x_e^* - x_m|$, $|y_e^* - y_m|$ indicate the typical errors that are available for feedback control while the tracking errors from the end-effector side indicate the manufacturing performance. The contouring error quantitatively determines the final manufacturing accuracy for the biaxial contouring applications. The control efforts of controllers can be represented by integrating the absolute value of the current inputs during the process. These metrics are summarised in Table 1 to provide an insight of performance comparison between the benchmark controllers and the proposed control framework.

From Table 1, we can see that there are larger tracking error differences between the actuator side and end-effector side on Y-axis than the X-axis for all three control methods. This is due to the large position discrepancy Δy_e on Y-axis as discussed in the model validation section. The LQR achieves the smallest X-axis tracking errors on both actuator and end-effector sides, however, this is at the cost of the highest control effort among the three methods with 15.2701 A. The LQR computes the optimal control input without the consideration of the input constraints, resulting in a control input in

TABLE 1. Contouring performance comparison.

	Cascaded	LQR	Proposed approach
$\|x_e^* - x_m\|_\infty$	1.6845	0.3832	1.1856
$\|x_e^* - x_e\|_\infty$	1.6846	0.3829	1.1856
$\|y_e^* - y_m\|_\infty$	0.2998	1.9092	0.0505
$\|y_e^* - y_e\|_\infty$	1.0311	2.6982	0.8596
$\int \|i_x\| dt$	2.7175	15.2701	3.9268
$\int \|i_y\| dt$	7.5869	15.4098	7.4425
Contouring error	1.4555	2.5960	1.3308

Note: the unit of these errors is mm, unit of the control input is A.

characteristics similar to bang-bang control for the investigated system with input saturation. This frequent changing control input of LQR enlarges the tracking error on the Y-axis as 2.698 mm and 1.909 mm for the end-effector and actuator side, leading to the largest contouring error 2.596 mm among the three methods.

The proposed controller achieves smaller tracking errors on X-axis for both the actuator and end-effector sides compared to the conventional cascaded controller. This reduced tracking error is achieved by the introduced ESO structure with slightly higher control input for the proposed control method with 3.9268 A compared to the cascaded controller with 2.717 A. A more obvious improvement can be seen from the tracking errors on Y-axis by comparing the proposed approach with benchmark controllers. The smallest tracking errors as 0.0505 mm on the actuator side and 0.8596 mm on the end-effector side are achieved by the proposed method with the lowest control effort 7.4425 A, which demonstrates the effectiveness of the MPC based controller. Although the largest tracking errors on X-axis is formed by the cascaded controller, it produces the average contouring error based on the moderate control inputs.

In summary, the LQR based method uses the aggressive control effort but the resulting oscillation on the Y-axis deteriorates the final contouring performance. The proposed control framework achieves a promising contouring performance by explicitly considering the operating constraints as well as the coupled and rotation dynamics.

V. CONCLUSION

In this work, the modelling and contouring control for an industrial biaxial machine in a cantilever beam structure is investigated. The derivation of the proposed physics-based model serves as a good example for modelling systems with dominant fundamental vibration frequency, and the modelling process can be easily extended for other biaxial machines such as dual-drive machines. The proposed control architecture based on ESO and MPC offers a framework for dealing with states coupling systems in the contouring control field. The results show that the proposed model-based approach outperforms the conventional cascaded control and LQR control in both contouring accuracy and vibration reduction. Future work may involve the development of the end-effector position measurement and exploration of experiments on the industrial machine.

$$A(\bar{x}_m) = \begin{bmatrix} 1 & T_s & 0 & 0 \\ 0 & 1 & \dfrac{6k_t(2M_x\bar{x}_m + M_bL_b)T_s}{\Lambda} & \dfrac{6c_t(2M_x\bar{x}_m + M_bL_b)T_s}{\Lambda} \\ 0 & 0 & 1 & \dfrac{T_s}{\Lambda} \\ 0 & 0 & \dfrac{-12k_t(M_x + M_y + M_b)T_s}{\Lambda} & 1 + \dfrac{-12c_s(M_x + M_y + M_b)T_s}{\Lambda} \end{bmatrix},$$

$$B(\bar{x}_m) = \begin{bmatrix} 0 \\ \dfrac{\left(4M_bL_b^2 + 12M_x\bar{x}_m^2\right)T_s}{\Lambda} \\ 0 \\ \dfrac{(-12M_x\bar{x}_m - 6M_bL_b)\,T_s}{\Lambda} \end{bmatrix}, \quad E(\bar{x}_m) = \begin{bmatrix} 0 & 0 \\ \dfrac{\left(4M_bL_b^2 + 12M_x\bar{x}_m^2\right)T_s}{\Lambda} & \dfrac{(-12M_x\bar{x}_m - 6M_bL_b)\,T_s}{\Lambda} \\ 0 & 0 \\ \dfrac{(-12M_x\bar{x}_m - 6M_bL_b)\,T_s}{\Lambda} & \dfrac{12(M_x + M_y + M_b)T_s}{\Lambda} \end{bmatrix},$$

APPENDIX A
COEFFICIENT OF MATRICES IN CONTROL-ORIENTED MODEL

The explicit form of the coefficient matrix in Eq. (23) is given at the top of the page, where $\Lambda \triangleq M_b^2L_b^2 + 4M_bL_b^2(M_x + M_y) + 12M_x\bar{x}_m(M_b\bar{x}_m + M_y\bar{x}_m - M_bL_b)$.

ACKNOWLEDGMENT

We would like to thank Dr. Lu Gan from ANCA Motion, Australia for the support of the experiments.

REFERENCES

[1] K. S. Sollmann, M. K. Jouaneh, and D. Lavender, "Dynamic modeling of a two-axis, parallel, H-frame-type XY positioning system," *IEEE/ASME Trans. Mechatronics*, vol. 15, no. 2, pp. 280–290, Apr. 2010.

[2] M. Yuan, C. Manzie, L. Gan, M. Good, and I. Shames, "Modelling and contouring error bounded control of a biaxial industrial gantry machine," in *Proc. IEEE Conf. Control Technol. Appl. (CCTA)*, Aug. 2019, pp. 388–393.

[3] Z. Wang, C. Hu, and Y. Zhu, "Accelerated iteration algorithm based contouring error estimation for multiaxis motion control," *IEEE/ASME Trans. Mechatronics*, vol. 27, no. 1, pp. 452–462, Feb. 2022.

[4] W. Wang, J. Ma, Z. Cheng, X. Li, C. De Silva, and T. H. Lee, "Global iterative sliding mode control of an industrial biaxial gantry system for contouring motion tasks," *IEEE/ASME Trans. Mechatronics*, early access, Jul. 14, 2021, doi: 10.1109/TMECH.2021.3096601.

[5] J. Ma, S.-L. Chen, N. Kamaldin, C. S. Teo, A. Tay, A. Al Mamun, and K. K. Tan, "Integrated mechatronic design in the flexure-linked dual-drive gantry by constrained Linear–Quadratic optimization," *IEEE Trans. Ind. Electron.*, vol. 65, no. 3, pp. 2408–2418, Mar. 2018.

[6] H.-K. Park, S.-S. Kim, J.-M. Park, T.-Y. Cho, and D. Hong, "Dynamics of dual-drive servo mechanism," in *Proc. ISIE. IEEE Int. Symp. Ind. Electron.*, Jan. 2001, pp. 1996–2000. [Online]. Available: http://ieeexplore.ieee.org/document/932020/

[7] Z. Mohamed and M. O. Tokhi, "Command shaping techniques for vibration control of a flexible robot manipulator," *Mechatronics*, vol. 14, no. 1, pp. 69–90, Feb. 2004. [Online]. Available: https://linkinghub.elsevier.com/retrieve/pii/S0957415803000138

[8] W. He and S. S. Ge, "Vibration control of a flexible beam with output constraint," *IEEE Trans. Ind. Electron.*, vol. 62, no. 8, pp. 5023–5030, Aug. 2015. [Online]. Available: http://ieeexplore.ieee.org/document/7031915/

[9] M. Yuan, C. Manzie, M. Good, I. Shames, L. Gan, F. Keynejad, and T. Robinette, "A review of industrial tracking control algorithms," *Control Eng. Pract.*, vol. 102, Sep. 2020, Art. no. 104536, doi: 10.1016/j.conengprac.2020.104536.

[10] M. Kumar, B. Mukherjee, K. B. M. M. Swamy, and S. Sen, "A novel design for enhancing the sensitivity of a capacitive MEMS device," *J. Microelectromech. Syst.*, vol. 27, no. 4, pp. 656–666, Aug. 2018.

[11] P. R. Ouyang, V. Pano, J. Tang, and W. H. Yue, "Position domain nonlinear PD control for contour tracking of robotic manipulator," *Robot. Comput.-Integr. Manuf.*, vol. 51, pp. 14–24, Jun. 2018.

[12] M. Azimi and E. Farzaneh Joubaneh, "Dynamic modeling and vibration control of a coupled rigid-flexible high-order structural system: A comparative study," *Aerosp. Sci. Technol.*, vol. 102, Jul. 2020, Art. no. 105875, doi: 10.1016/j.ast.2020.105875.

[13] Y. Altintas, A. Verl, C. Brecher, L. Uriarte, and G. Pritschow, "Machine tool feed drives," *CIRP Ann.*, vol. 60, no. 2, pp. 779–796, 2011, doi: 10.1016/j.cirp.2011.05.010.

[14] H. N. Rahimi and M. Nazemizadeh, "Dynamic analysis and intelligent control techniques for flexible manipulators: A review," *Adv. Robot.*, vol. 28, no. 2, pp. 63–76, 2014.

[15] C. F. Castillo-Berrio and V. Feliu-Batlle, "Vibration-free position control for a two degrees of freedom flexible-beam sensor," *Mechatronics*, vol. 27, pp. 1–12, Apr. 2015, doi: 10.1016/j.mechatronics.2015.01.005.

[16] Q. Zhang, X. Zhao, L. Liu, and T. Dai, "Adaptive sliding mode neural network control and flexible vibration suppression of a flexible spatial parallel robot," *Electronics*, vol. 10, no. 2, p. 212, Jan. 2021. [Online]. Available: https://www.mdpi.com/2079-9292/10/2/212

[17] W. Symens, H. van Brussel, and J. Swevers, "Gain-scheduling control of machine tools with varying structural flexibility," *CIRP Ann.*, vol. 53, no. 1, pp. 321–324, 2004. [Online]. Available: http://linkinghub.elsevier.com/retrieve/pii/S0007850607607070

[18] L. Lu, Z. Chen, B. Yao, and Q. Wang, "A two-loop performance-oriented tip-tracking control of a linear-motor-driven flexible beam system with experiments," *IEEE Trans. Ind. Electron.*, vol. 60, no. 3, pp. 1011–1022, Mar. 2013. [Online]. Available: http://ieeexplore.ieee.org/document/6153370/

[19] C. Li, B. Yao, and Q. Wang, "Modeling and synchronization control of a dual drive industrial gantry stage," *IEEE/ASME Trans. Mechatronics*, vol. 23, no. 6, pp. 2940–2951, Dec. 2018. [Online]. Available: https://ieeexplore.ieee.org/document/8486733/

[20] Y. Koren and C.-C. Lo, "Variable-gain cross-coupling controller for contouring," *CIRP Ann.*, vol. 40, no. 1, pp. 371–374, Jan. 1991.

[21] C. Hu, B. Yao, and Q. Wang, "Coordinated adaptive robust contouring controller design for an industrial biaxial precision gantry," *IEEE/ASME Trans. Mechatron.*, vol. 15, no. 5, pp. 728–735, Oct. 2010. [Online]. Available: http://ieeexplore.ieee.org/document/5338034/

[22] M. Corapsiz and K. Erenturk, "Trajectory tracking control and contouring performance of three dimensional CNC," *IEEE Trans. Ind. Electron.*, vol. 63, no. 4, pp. 2212–2220, Apr. 2016. [Online]. Available: http://ieeexplore.ieee.org/document/7360158/

[23] W.-H. Chen, J. Yang, L. Guo, and S. Li, "Disturbance-observer-based control and related nethods—An overview," *IEEE Trans. Ind. Electron.*, vol. 63, no. 2, pp. 1083–1095, Feb. 2016.

[24] E. Sariyildiz, S. Hangai, T. Uzunovic, T. Nozaki, and K. Ohnishi, "Stability and robustness of the disturbance observer-based motion control systems in discrete-time domain," *IEEE/ASME Trans. Mechatronics*, vol. 26, no. 4, pp. 2139–2150, Aug. 2021.

[25] K. K. Tan, T. H. Lee, H. F. Dou, S. J. Chin, and S. Zhao, "Precision motion control with disturbance observer for pulsewidth-modulated-driven permanent-magnet linear motors," *IEEE Trans. Magn.*, vol. 39, no. 3, pp. 1813–1818, May 2003. [Online]. Available: http://ieeexplore.ieee.org/document/1198376/

[26] Y. X. Su, C. H. Zheng, and B. Y. Duan, "Automatic disturbances rejection controller for precise motion control of permanent-magnet synchronous motors," *IEEE Trans. Ind. Electron.*, vol. 52, no. 3, pp. 814–823, Jun. 2005. [Online]. Available: http://ieeexplore.ieee.org/document/1435693/
[27] J. Solsona, M. I. Valla, and C. Muravchik, "Nonlinear control of a permanent magnet synchronous motor with disturbance torque estimation," *IEEE Trans. Energy Convers.*, vol. 15, no. 2, pp. 163–168, Jun. 2000. [Online]. Available: http://ieeexplore.ieee.org/document/866994/
[28] X. Sun, Y. Zhang, G. Lei, Y. Guo, and J. Zhu, "An improved deadbeat predictive stator flux control with reduced-order disturbance observer for in-wheel PMSMs," *IEEE/ASME Trans. Mechatronics*, early access, Mar. 26, 2021, doi: 10.1109/TMECH.2021.3068973.
[29] W.-S. Huang, C.-W. Liu, P.-L. Hsu, and S.-S. Yeh, "Precision control and compensation of servomotors and machine tools via the disturbance observer," *IEEE Trans. Ind. Electron.*, vol. 57, no. 1, pp. 420–429, Jan. 2010. [Online]. Available: http://ieeexplore.ieee.org/document/5291793/
[30] C. J. Kempf and S. Kobayashi, "Disturbance observer and feedforward design for a high-speed direct-drive positioning table," *IEEE Trans. Control Syst. Technol.*, vol. 7, no. 5, pp. 513–526, Sep. 1999. [Online]. Available: http://ieeexplore.ieee.org/document/784416/
[31] Z. Jamaludin, H. Van Brussel, and J. Swevers, "Friction compensation of an XY feed table using friction-model-based feedforward and an inverse-model-based disturbance observer," *IEEE Trans. Ind. Electron.*, vol. 56, no. 10, pp. 3848–3853, Oct. 2009. [Online]. Available: http://ieeexplore.ieee.org/document/4808130/
[32] P. J. Serkies and K. Szabat, "Application of the MPC to the position control of the two-mass drive system," *IEEE Trans. Ind. Electron.*, vol. 60, no. 9, pp. 3679–3688, Sep. 2013. [Online]. Available: http://ieeexplore.ieee.org/document/6241426/
[33] E. J. Fuentes, C. A. Silva, and J. I. Yuz, "Predictive speed control of a two-mass system driven by a permanent magnet synchronous motor," *IEEE Trans. Ind. Electron.*, vol. 59, no. 7, pp. 2840–2848, Jul. 2012. [Online]. Available: http://ieeexplore.ieee.org/document/5783930/
[34] M. Yuan, C. Manzie, M. Good, I. Shames, L. Gan, F. Keynejad, and T. Robinette, "Error-bounded reference tracking MPC for machines with structural flexibility," *IEEE Trans. Ind. Electron.*, vol. 67, no. 10, pp. 8143–8154, Oct. 2020.
[35] B.-Z. Guo and Z.-L. Zhao, "On the convergence of an extended state observer for nonlinear systems with uncertainty," *Syst. Control Lett.*, vol. 60, pp. 420–430, Jun. 2011. [Online]. Available: https://linkinghub.elsevier.com/retrieve/pii/S016769111100065X
[36] D. Q. Mayne, J. B. Rawlings, C. V. Rao, and P. O. M. Scokaert, "Constrained model predictive control: Stability and optimality," *Automatica*, vol. 36, no. 6, pp. 789–814, 2000. [Online]. Available: http://linkinghub.elsevier.com/retrieve/pii/S0005109899002149
[37] A. Visioli and G. Legnani, "On the trajectory tracking control of industrial SCARA robot manipulators," *IEEE Trans. Ind. Electron.*, vol. 49, no. 1, pp. 224–232, Feb. 2002. [Online]. Available: http://ieeexplore.ieee.org/document/982266/

MENG YUAN received the B.Sc. degree in automation and the M.Sc. degree in control theory and control engineering from Northeastern University, China, in 2013 and 2015, respectively, and the Ph.D. degree in electrical and electronic engineering from the University of Melbourne, Australia, in 2020.

He is currently a Research Fellow with the Rehabilitation Research Institute of Singapore, Nanyang Technological University, Singapore. He is also working on several projects with Fuzhou University, China. His research interests include modeling, model-based and model-free control for rehabilitation robots, and industrial machines. He was a recipient of the Keynote Paper Award at the 25th Chinese Process Control Conference.

LEI LI received the bachelor's and Ph.D. degrees in mechanical and aerospace engineering from Nanyang Technological University, Singapore, in 2010 and 2016, respectively.

He is currently a Senior Research Fellow with the Rehabilitation Research Institute of Singapore, Nanyang Technological University. His research interests include robot mechanism design, control, and human–robot interaction. He has ten year's of experience working on rehabilitation and assistive robotics and developed a wide range of assistive robotics covering the function of arm movements, walking, balance, driving, and transferring.

ZHEZHUANG XU (Member, IEEE) received the B.Eng. degree in automation from Xiamen University, Xiamen, China, in 2005, the M.Eng. degree in measuring and testing technologies and instruments from Jiangsu University, Zhenjiang, China, in 2008, and the Ph.D. degree in control science and engineering from Shanghai Jiao Tong University, Shanghai, China, in 2012.

He joined the School of Electrical Engineering and Automation, Fuzhou University, Fuzhou, China, in 2012, where he is currently a Full Professor. He is currently the Director of the Public Platform of Industrial Big Data Application, Fujian Provincial Commission of Economy and Information Technology. He has authored and coauthored over 50 refereed international journals and conference papers. His research interests include wireless communication and big data analysis in industrial manufacturing.